[Supporting information]

Size-Controlled Self-Assembly of Superparamagnetic Polymersomes

Robert J. Hickey,[1] Jason Koski,[2] Xin Meng,[3] Robert A. Riggleman,[2] Peijun Zhang,[3] and So-Jung Park[1,4,]*

[1]Department of Chemistry, University of Pennsylvania, 231 S South 34th Street, Philadelphia, PA 19104, [2]Department of Chemical and Biomedical Engineering, University of Pennsylvania, 220 S South 33rd Street, Philadelphia, PA 19104, [3]Department of Structural Biology, University of Pittsburgh School of Medicine, 3501 5th Avenue, Pittsburgh, PA 15260, and [4]Department of Chemistry and Nano Science, Global Top 5 Program, Ewha Womans University, 52 Ewhayeodae-gil, Seodaemun-gu, Seoul, 120-750, Korea

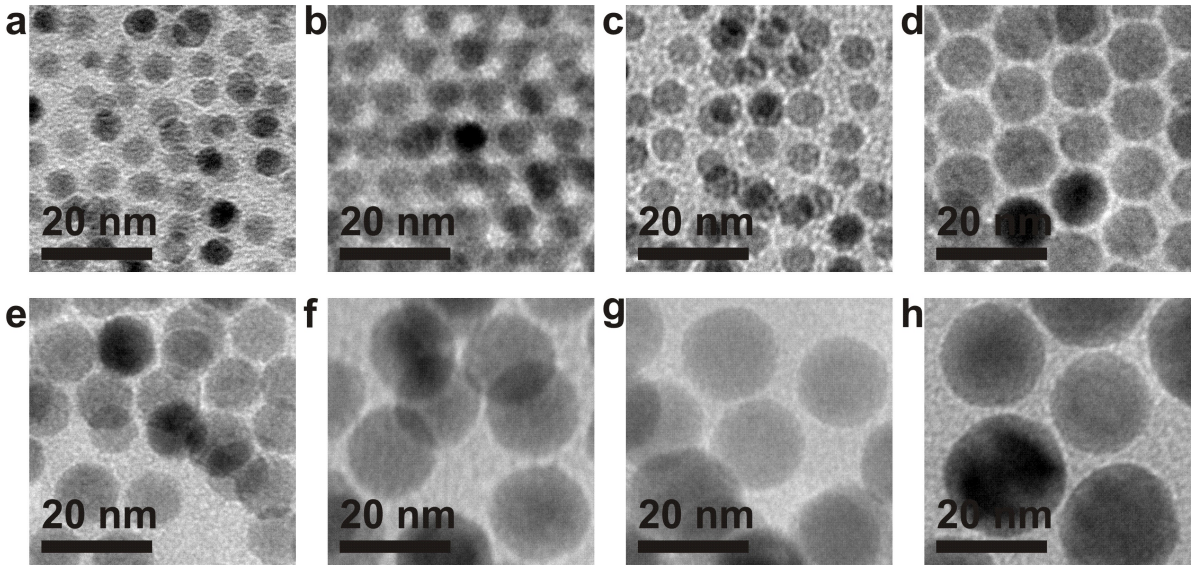

Figure S1: TEM images of various sized iron oxide nanoparticles used in the study. (a) 5.6 $\pm$ 0.5 nm, (b) 5.8 $\pm$ 0.7 nm, (c) 6.4 $\pm$ 0.5 nm, (d) 9.9 $\pm$ 0.8 nm, (e) 10.8 $\pm$ 0.7 nm, (f) 15.5 $\pm$ 0.8 nm, (g) 16.3 $\pm$ 1.1 nm, and (h) 19.9 $\pm$ 1.3.

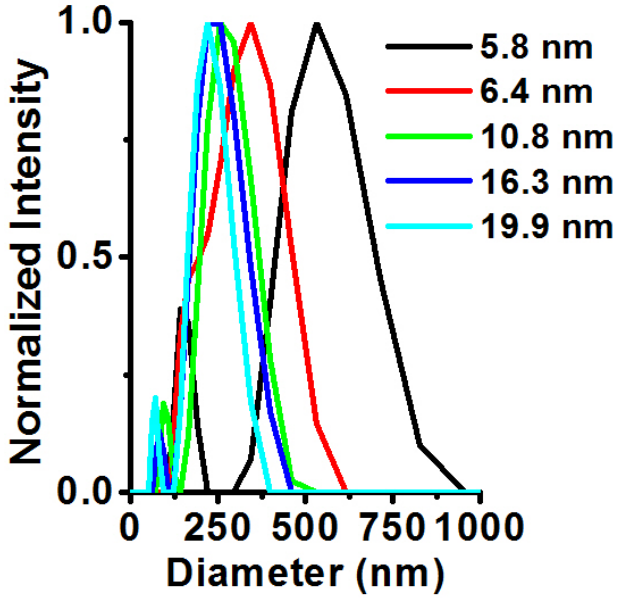

Figure S2: Normalized DLS data for magneto-polymersomes formed with a series of different sized nanoparticles at 25 np wt % using the polymer PAA_{38}-*b*-PS_{73}.

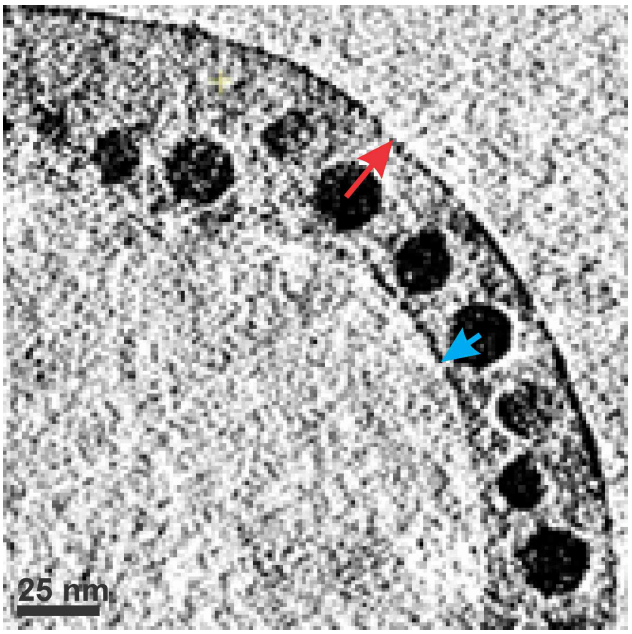

Figure S3: Distances from the middle of the 16.3 nm iron oxide particle to the outer (red arrow) or inner (blue arrow) edge of the vesicle membrane were measured to be 20.2 $\pm$ 4.5 nm and 13.6 $\pm$ 2.2 nm, respectively. Only monolayer regions were used for the measurements.

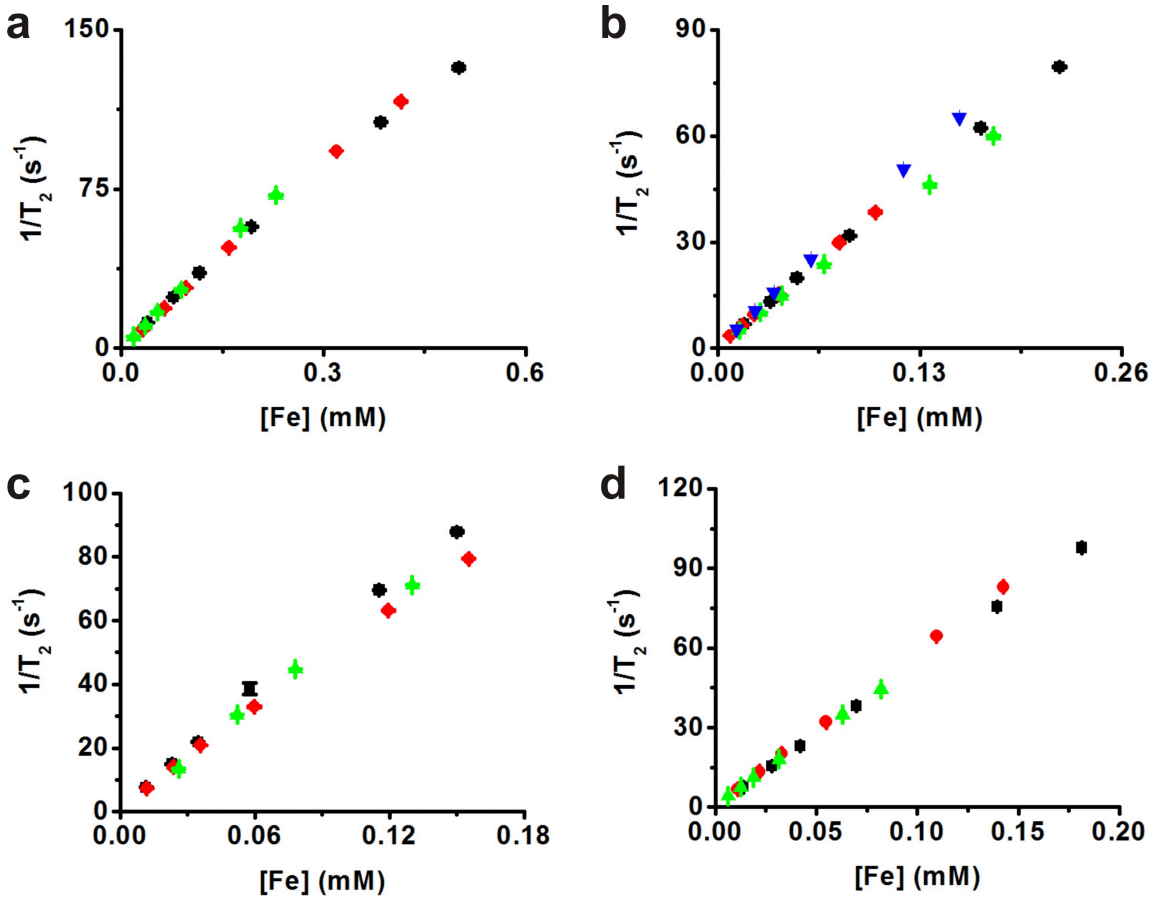

Figure S4: Inverse transverse relaxation times ($1/T_2$) *versus* the iron molar concentration [Fe] of magneto-polymersomes assembled with different sized iron oxide nanoparticles: (a) 5.6 nm, (b) 6.4 nm, (c) 10.8 nm, and (d) 15.5 nm. Different colored dots correspond to different measurements.

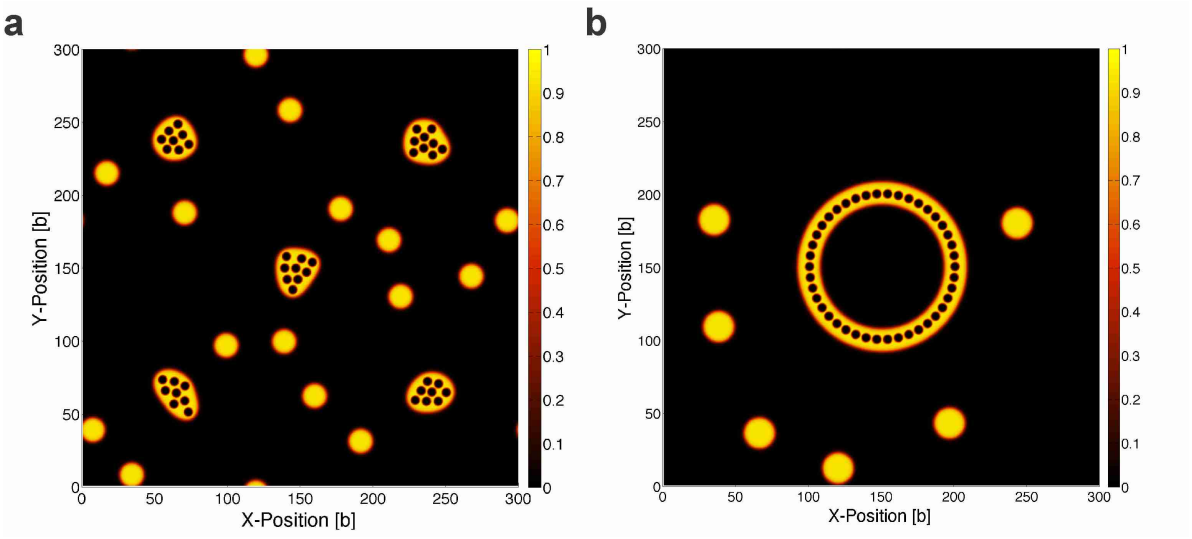

Figure S5: Sample configurations of the SCFT calculations for $f_A = 0.3$ and $R_p = 1.34R_g$, where the system forms either micelles (a) or a polymersome (b). The color bar refers to the local volume fraction of the B (hydrophobic) block of the diblock copolymer. All of the nanoparticles are visible as spheres imbedded in B-rich phases. The micelle configuration in (a) is an example of a calculation that was initialized to form five micelles.

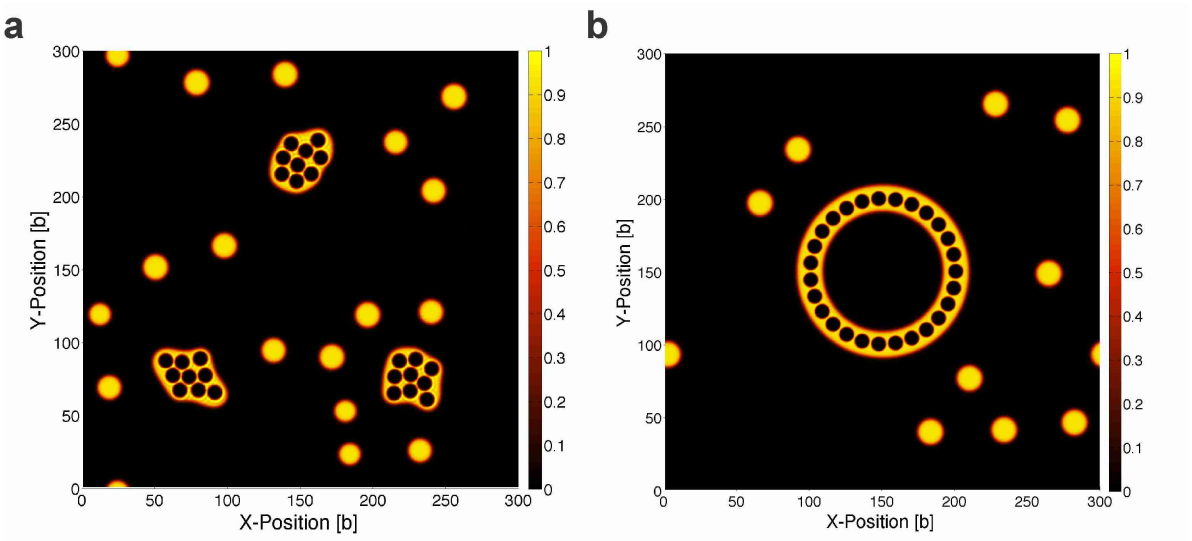

Figure S6: Similar calculations as Figure S5 carried out for larger nanoparticles having a radius of $R_p = 2.24R_g$ forming either micelles (a) or polymersomes (b). In the micelle calculations, the nanoparticles were biased to form three individual micelles.

Hybrid particle-field simulations

We have employed a formulation of polymer field theory called the hybrid particle-field (HPF) theory that enables the incorporation of discrete nanoparticles into a matrix of polymers and solvent.[1] Here we briefly describe the essential points in the derivation and implementation of the HPF model employed here. Following previous work,[2] we assume that each particle in our simulation represents a collection of atomistic segments (either solvent molecules or polymer monomers) that are Gaussian distributed over a small volume whose length scale is given by the statistical segment size of the polymer, b. With this picture, the particle density of the solvent is given by

$$\hat{\rho}_S(\mathbf{r}) = \sum_i^{n_S} \Gamma(\mathbf{r}-\mathbf{r}_i) \tag{1}$$

where

$$\Gamma(\mathbf{r}) = \left(\frac{1}{2\pi b^2}\right)^{3/2} e^{-|\mathbf{r}|^2/2b^2}. \tag{2}$$

Our diblock polymer chains are modeled as discrete Gaussian chains consisting of $N = N_A + N_B$ total beads. The density of components A and B due to the diblock are given by

$$\hat{\rho}_{DK} = \sum_i^{n_D}\sum_j^{N_K} \Gamma(\mathbf{r}-\mathbf{r}_{i,j}), \tag{3}$$

where n_D is the number of diblocks in the system and K represents either species A or B. For the sake of simplicity, we treat the solvent and the A block of the copolymer as chemically identical and label them generically as species A; our total A density is therefore $\hat{\rho}_A(\mathbf{r}) = \hat{\rho}_S(\mathbf{r}) + \hat{\rho}_{DA}(\mathbf{r})$, and our total B density is simply $\hat{\rho}_B(\mathbf{r}) = \hat{\rho}_{DB}(\mathbf{r})$.

The beads along the polymer backbone are connected via harmonic springs given by the po-

tential

$$\beta U_0 = \sum_i^{n_D} \sum_j^{N-1} \beta u_{bond}(|\mathbf{r}_{i,j} - \mathbf{r}_{i,j+1}|), \tag{4}$$

$$\beta u_{bond}(r) = \frac{N}{4R_g^2} r^2, \tag{5}$$

where $R_g = b\sqrt{N/6}$ is the unperturbed radius of gyration of the polymer chain. The A and B segments interact with a simple local interaction of the form

$$\beta U_1 = \frac{\chi_{AB}}{\rho_0} \int d\mathbf{r}\, \hat{\rho}_A(\mathbf{r})\, \hat{\rho}_B(\mathbf{r}), \tag{6}$$

where χ_{AB} is a Flory "chi" parameter that governs the strength of the repulsive interaction segments A and B, and ρ_0 is the average total segment density without nanoparticles, $\rho_0 = (n_S + n_D N)/V$.

The nanoparticles are incorporated as cavity functions that exclude the volume of the polymer segments and solvent molecules, and the density of the nanoparticles is given by

$$\hat{\rho}_P(\mathbf{r}) = \sum_i^{n_P} h(|\mathbf{r} - \mathbf{r}_i|), \tag{7}$$

where $h(r)$ is the cavity function that describes how the density of nanoparticle i is distributed around its center located at $\mathbf{r}_i$. The functional form used for $h(r)$ is chosen to take the form of a complimentary error function,

$$h(r) = \rho_0 \frac{1}{2} \mathrm{erfc}\left[\frac{\mathrm{r} - \mathrm{R_p}}{\xi}\right], \tag{8}$$

which goes smoothly from the average total density ρ_0 to 0 over an interface whose width is governed by a numerical parameter, ξ, and the radius of which is given by R_p.

The nanoparticles also interact with segments A and B through a simple Flory-type repulsion, whose strength is governed by χ_{PA} and χ_{PB}, respectively. The form of this potential is

identical to that given in Eq. Figure S6,

$$\beta U_2 = \frac{\chi_{PK}}{\rho_0} \int d\mathbf{r}\, \hat{\rho}_K(\mathbf{r})\, \hat{\rho}_P(\mathbf{r}). \tag{9}$$

The final ingredient that we need for our model system is an incompressibility constraint, which fixes the density at each point in space to be ρ_0.

Combining the ingredients described above, we write our partition function for this system and trace through the exact Hubbard-Stratonovich transformation from a particle to a field theory following techniques that are well-established in the literature.[1,3,4] This leads to the partition function that is given by

$$\mathscr{Z} = z_0 \int \mathscr{D}w_+ \int \mathscr{D}w_- \int d\mathbf{r}^{n_P}\, e^{\mathscr{H}(\mathbf{r}^{n_P};[w_+,w_-])}, \tag{10}$$

where w_+ and w_- are chemical potential fields that govern the local incompressibility and local phase separation, respectively, and z_0 is the numerical prefactor that contains the thermal de Broglie wavelengths and normalization constants that arise from the particle-to-field transformation. $\mathscr{H}$ is the effective Hamiltonian governing the system, which is given by

$$\begin{aligned} \mathscr{H}(\mathbf{r}^{n_P};[w_+,w_-]) = & \int d\mathbf{r} \left[\frac{\rho_0}{\chi_{AB}} w_-(\mathbf{r})^2 - i w_+(\mathbf{r}) \{\rho_0 - \hat{\rho}_P(\mathbf{r})\} \right] \\ & - n_S \ln Q_S[w_A] - n_D \ln Q_D[w_A, w_B]. \end{aligned} \tag{11}$$

Here, i is the imaginary unit $i = \sqrt{-1}$, and w_A and w_B are the effective chemical potential fields observed by species A and B, which are given by

$$w_A(\mathbf{r}) = (\Gamma * [i w_+ - w_- + \frac{\chi_{AP}}{\rho_0} \hat{\rho}_P])(\mathbf{r}) \tag{12}$$

$$w_B(\mathbf{r}) = (\Gamma * [i w_+ + w_- + \frac{\chi_{BP}}{\rho_0} \hat{\rho}_P])(\mathbf{r}), \tag{13}$$

where the notation $(f * g)(\mathbf{r})$ indicates a convolution of the functions f and g. Q_S in Eq. Figure S6

above is the partition function of a single solvent molecule in the external field w_A and is given by

$$Q_S = \frac{1}{V}\int d\mathbf{r} e^{-w_A(\mathbf{r})}. \tag{14}$$

The density of the solvent is given by the operator

$$\tilde{\rho}_S(\mathbf{r}) = -\frac{n_S}{Q_S}\frac{\delta Q_S}{\delta w_A} = \frac{n_S}{Q_S V} e^{-w_A(\mathbf{r})}. \tag{15}$$

Obtaining the partition function and density operator of the diblock copolymers is the most computationally demanding aspect of the polymer field theory, as it requires iterating a Chapman-Kolmogorov equation[3] to obtain the chain propagators as

$$q(\mathbf{r}, j; [w_A, w_B]) = \begin{cases} e^{-w_A(\mathbf{r})} \int d\mathbf{r}' c_0 e^{-\beta u_{bond}(|\mathbf{r}-\mathbf{r}'|)} q(\mathbf{r}', j-1; [w_A, w_B]) & 1 \le j \le N_A \\ e^{-w_B(\mathbf{r})} \int d\mathbf{r}' c_0 e^{-\beta u_{bond}(|\mathbf{r}-\mathbf{r}'|)} q(\mathbf{r}', j-1; [w_A, w_B]) & N_A < j \le N \end{cases} \tag{16}$$

where the convolution of $e^{-\beta u_{bond}}$ with the partition function of the previous monomer is efficiently evaluated using a Fourier transform, inverse Fourier transform pair, and the initial condition for the propagator (where $j = 1$) is given by $q(\mathbf{r}, 0; [w_A]) = e^{-w_A(\mathbf{r})}$, and c_0 is the normalization constant for the bond transition probability. The partition function of a single diblock chain Q_D appearing in Eq. Figure S6 is then calculated as

$$Q_D[w_A, w_B] = \frac{1}{V}\int d\mathbf{r}\, q(\mathbf{r}, N; [w_A, w_B]). \tag{17}$$

To calculate the segment densities of the diblock copolymers, we need the complimentary propagator $q^\dagger(\mathbf{r}, j)$ built up by iterating a Chapman-Kolmogorov equation that begins from the B end of the diblock as

$$q^\dagger(\mathbf{r}, j; [w_A, w_B]) = \begin{cases} e^{-w_B(\mathbf{r})} \int d\mathbf{r}'\, c_0\, e^{-\beta u_{bond}(|\mathbf{r}-\mathbf{r}'|)}\, q^\dagger(\mathbf{r}', j-1; [w_A, w_B]) & 1 \le j \le N_B \\ e^{-w_A(\mathbf{r})} \int d\mathbf{r}'\, c_0\, e^{-\beta u_{bond}(|\mathbf{r}-\mathbf{r}'|)}\, q^\dagger(\mathbf{r}', j-1; [w_A, w_B]) & N_B < j \le N \end{cases} \tag{18}$$

with the initial condition $q^{\dagger}(\mathbf{r},1;[w_B]) = e^{-w_B(\mathbf{r})}$. The segment density is then calculated as the product of the propagators arising from growing the chain in either direction

$$\tilde{\rho}_{DA}(\mathbf{r}) = \sum_{j=1}^{N_A} q(\mathbf{r},j;[w_A,w_B])\, e^{w_A(\mathbf{r})}\, q^{\dagger}(\mathbf{r},N-j;[w_A,w_B]) \tag{19}$$

and

$$\tilde{\rho}_{DB}(\mathbf{r}) = \sum_{j=N_A+1}^{N} q(\mathbf{r},j;[w_A,w_B])\, e^{w_B(\mathbf{r})}\, q^{\dagger}(\mathbf{r},N-j;[w_A,w_B]). \tag{20}$$

The extra factor of e^{w_K} that arises in each expression is due to an extra factor of e^{-w_K} when multiplying the two propagators together.

Mean-field approximation and numerical approach

Following previous implementations of the HPF approach,[1,5] we evaluate our theory under a mean-field approximation where we assume that the partition function is dominated by the values of the fields and particle configurations that minimize the free energy of the system. Under this approximation, the partition function becomes

$$\mathscr{Z} \approx z_0\, e^{-\mathscr{H}(\mathbf{r}^{nP};[w_+^*,w_-^*])}, \tag{21}$$

where the * indicates the value of w_+ and w_- that minimize $\mathscr{H}$. Within this approximation, $\mathscr{H} = F$, the Helmholtz free energy, to within a constant. In the text we present the values of $\mathscr{H}$ from the minimized configurations as well as the average entropy of the polymer chains, S/n_D, calculated as

$$S/n_D = \log Q_D + \frac{1}{n_D}\int d\mathbf{r}\,[w_A\tilde{\rho}_{DA}(\mathbf{r}) + w_B\tilde{\rho}_{DB}(\mathbf{r})] \tag{22}$$

for the values of the densities and fields at the mean-field configuration. All calculations presented in this work were performed using the pseudo-spectral approach in a simulation box that was $134.16R_g \times 134.16R_g$ in size with $N_x = 405$ grid points in each direction. The total chain length

was fixed at $N = 30$, and we varied the amount of N_A relative to N_B to vary the composition of the chains. Two nanoparticle radii were considered, $R_p = 2.24R_g$ and $1.34R_g$, and the number of nanoparticles was $n_P = 27$ and $n_P = 42$ in each case, respectively. The amount of polymer in all cases was held constant at $n_D = 264$.

Vesicle calculations. The nanoparticles are placed in a circular configuration and held fixed at their initial location. This approach is inspired by the tomography data, which show that the larger nanoparticles are regularly ordered in the polymersome leaflets. We then randomly initialize the w_- field, which controls the segregation between the A and B segments, while initializing the w_+ field to zero. From this point, we employ the first-order semi-empirical splitting approach of Ceniceros and Fredrickson[6] to find the mean-field configuration of w_+ and w_-.

For the nanoparticle-free polymersome calculations, we bias the initial configuration of the w_- field such that all of the hydrophobic B polymer segments form a circular polymersome of a given radius. Next, we relax the fields using the same algorithm as the case where the particles are present. Without particles, the size of the polymersome is free to adapt to its preferred radius without forming coexisting micelles in the solution.

Micelle and cluster calculations. Several approaches were tried to generate nanoparticle-loaded micelles, and each approach gave the same qualitative trend as that presented in the main text. TEM tomography data show that multiple nanoparticles are embedded in large micelles; therefore, we designed a series of calculations to replicate the experimental observations. First, for a given nanoparticle size, we used the same number of nanoparticles as in the polymersome calculations, and we chose to split the nanoparticles up into separate groups where the particles would be placed randomly near each other in clusters. Depending on the number of groups we chose, the number of nanoparticles per group could potentially vary. After choosing the number of groups and the initial particle positions, we again initialized w_- to a random field while w_+ was initialized to zero and minimized $\mathscr{H}$ with respect to both the field variables w_+ and w_- and the particle positions. Because the minimization with respect to particle positions is unique to the cluster calculations, we have verified that the trends we observe do not change qualitatively if we

leave the particles fixed at their initial configurations. Furthermore, we have verified that changing the number of particle clusters (and therefore the number of particles per cluster) does not alter our results.

For the nanoparticle-free micelle calculations, we simply initialized the w_- to random values while w_+ was initialized to zero and minimized $\mathscr{H}$. This leads to the rapid formation of micelles that are randomly dispersed throughout our simulation box.

References

(1) Sides, S. W.; Kim, B. J.; Kramer, E. J.; Fredrickson, G. H. Hybrid Particle-Field Simulations of Polymer Nanocomposites. *Phys. Rev. Lett.* **2006**, *96*, 250601.

(2) Riggleman, R. A.; Kumar, R.; Fredrickson, G. H. Investigation of the Interfacial Tension of Complex Coacervates Using Field Theoretic Simulations. *J. Chem. Phys.* **2012**, *136*, 024903.

(3) Fredrickson, G. H. *The Equilibrium Theory of Inhomogeneous Polymers*; Oxford University Press: New York, 2006.

(4) Matsen, M. W. The Standard Gaussian Model for Block Copolymer Melts. *J. Phys.: Condens. Matt.* **2001**, *14*, R21.

(5) Kim, S.; Cochran, E. Localization of Spherical Nanoparticles Within Lamellar AB Diblock Copolymer Melts Through Self-Consistent Field Theory. *Polymer* **2011**, 2328–2339.

(6) Ceniceros, H. D.; Fredrickson, G. H. Numerical Solution of Polymer Self-Consistent Field Theory. *Multiscale Model. Simul.* **2004**, *2*, 452.